Freire Gomez, J., Booker, J. D., & Mellor, P. (2015). Stress optimization of leaf-spring crossed flexure pivots for an active Gurney flap mechanism. In Proceedings SPIE 9433: Industrial and Commercial Applications of Smart Structures Technologies 2015. (Vol. 9433). SPIE. 10.1117/12.2082890

Stress optimization of leaf-spring crossed flexure pivots for an active Gurney flap mechanism

Jon Freire Gómez*[a], Julian D. Booker[a], Phil H. Mellor[b]
[a]Dept. of Mechanical Engineering, University of Bristol, Queen's Building, University Walk, Bristol, BS8 1TR, UK; [b]Dept. of Electrical and Electronic Engineering, University of Bristol, Merchant Venturers Building, Woodland Road, Bristol, BS8 1UB, UK

ABSTRACT

The EU's Green Rotorcraft programme is pursuing the development of a functional and airworthy Active Gurney Flap (AGF) for a full-scale helicopter rotor blade. Interest in the development of this 'smart adaptive rotor blade' technology lies in its potential to provide a number of aerodynamic benefits, which would in turn translate into a reduction in fuel consumption and noise levels. The AGF mechanism selected employs leaf-spring crossed flexure pivots. These provide important advantages over bearings as they are not susceptible to seizing and do not require maintenance (i.e. lubrication or cleaning). A baseline design of this mechanism was successfully tested both in a fatigue rig and in a 2D wind tunnel environment at flight-representative deployment schedules. For full validation, a flight test would also be required. However, the severity of the in-flight loading conditions would likely compromise the mechanical integrity of the pivots' leaf-springs in their current form. This paper investigates the scope for stress reduction through three-dimensional shape optimization of the leaf-springs of a generic crossed flexure pivot. To this end, a procedure combining a linear strain energy formulation, a parametric leaf-spring profile definition and a series of optimization algorithms is employed. The resulting optimized leaf-springs are proven to be not only independent of the angular rotation at which the pivot operates, but also linearly scalable to leaf-springs of any length, minimum thickness and width. Validated using non-linear finite element analysis, the results show very significant stress reductions relative to pivots with constant cross section leaf-springs, of up to as much as 30% for the specific pivot configuration employed in the AGF mechanism. It is concluded that shape optimization offers great potential for reducing stress in crossed flexure pivots and, consequently, for extending their fatigue life and/or rotational range.

Keywords: Active Gurney Flap, helicopter, flexure pivot, leaf-spring, shape optimization, minimum stress, fatigue life.

1. INTRODUCTION

1.1 Background

The performance of a helicopter is, to a great extent, determined by the aerodynamic behaviour of its main rotor. With the advent of Computational Fluid Dynamics (CFD), helicopter blades have undergone an important geometric optimization process, to the point of having virtually exhausted the scope for further aerodynamic improvement through changes in their geometry. At this stage, additional performance enhancement calls for morphing blades, i.e. smart adaptive structures capable of altering their shape while in service. In this context, the Green Rotorcraft[1] programme —which is part of the European Clean Sky Joint Technology Initiative (JTI)—, is pursuing the development of an Active Gurney Flap (AGF) for a full-scale helicopter rotor blade. Interest in the development of this 'smart adaptive rotor blade' technology lies in its potential to provide a number of aerodynamic benefits, which would in turn translate into a reduction in fuel consumption and noise levels.

The selection of the AGF concept under development was carried out following the methodology presented in a previous publication[2]. One of the main strengths of the concept selected lies in the employment of crossed flexure pivots in lieu of bearings. These provide a number of important advantages[3] over conventional joints as they are easily customisable, lightweight, maintenance free, backlash free —thus allowing precise control of position—, they do not suffer from frictional losses and they eliminate the possibility of a jam during motion.

*Jon.Freire@bristol.ac.uk; phone +44 (0) 117 331 5460

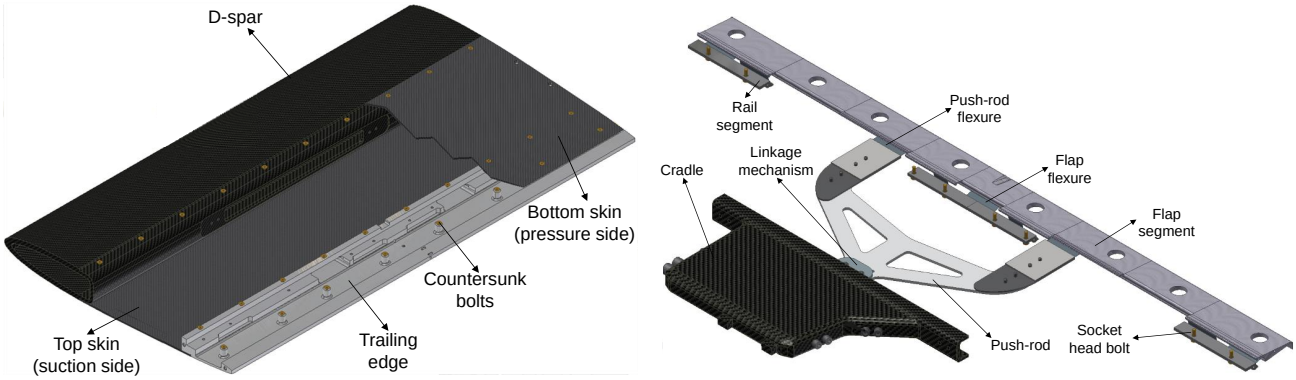

Figure 1. Left: Interrupted view of the blade aerofoil section with the AGF mechanism removed; Right: Isometric view of the AGF mechanism.

The chosen AGF concept consist essentially of: a cradle slotted in the D-spar of the blade which houses an actuator and a linkage/gearing mechanism, a push-rod that transfers the movement from the leading edge to the trailing edge, and a flap hinging on leaf-spring crossed flexure pivots which are, in turn, anchored to the blade structure.

A baseline design of said AGF concept (see Figs. 1 and 2) was successfully tested both in a fatigue rig and in a 2D wind tunnel environment at flight-representative deployment schedules (see refs[4,5] for more details). The system was designed to fit into a NACA 0012 aerofoil with a thickened trailing edge (3% chord thickness at 95% chord), with the flap sitting at 95% chord (chord=508mm).

In order to ensure as long as possible a fatigue life, a high endurance limit steel (CS95 (EN44)) was selected for the leaf-springs. Their thickness was chosen based on Eq. 18, which gives the maximum stress in any one crossed flexure pivot of constant cross section leaf-springs[6]. Therein, 'σ_e' is the endurance limit of the material in question ($\sigma_e \approx 550$MPa), 'λ' is a non-dimensional parameter defined in Section 2.1 ($\lambda \approx 1$), 'E' is Young's modulus (E≈200GPa), 't' is the thickness (t≈0.127mm), 'θ_z' is the angle rotated by the moving end of the leaf-springs ($\theta_z \approx \pm 5°$ in order to achieve a maximum flap deployment height of 1.3% chord) and 'L' is their active length (L≈9.4mm). It is important to note that the flap remains partially deployed when the flexures are at their neutral position as can be inferred from Fig. 2. In other words, the flexures have a -5° angular rotation when the flap is fully stowed inside the blade, whereas they reach a +5° angular rotation when the flap is fully deployed. This is to keep the absolute angle across which the flexures move —and by extension, the resulting stress— to a minimum.

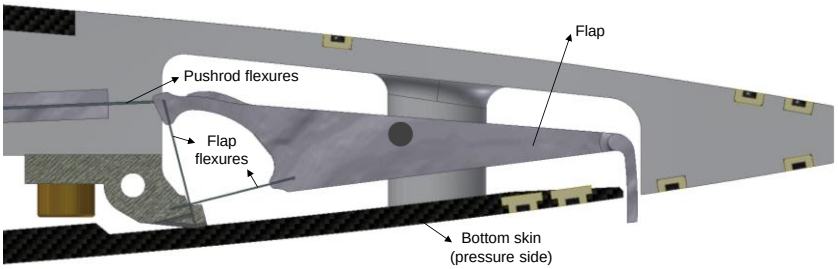

Figure 2. Detail of the AGF mechanism around the trailing edge region showing the crossed flexure pivots.

For full validation of the AGF system, a flight test would also be required. However, the severity of the in-flight loading conditions (in terms of centrifugal loads, blade deflections, etc.) would likely compromise the mechanical integrity of the leaf-springs as the design currently stands. Consequently, before the concept can be safely taken to flight test, design changes geared at reducing the maximum stress in the leaf-springs are needed.

Given a certain type of crossed flexure pivot configuration (i.e. λ), as well as a material (i.e. E) and an angle of rotation (i.e. θ_z), the logical way to reduce the maximum stress according to Eq. 18 is either to increase the active length of the leaf-springs 'L' or to reduce their thickness 't' (note that the width 'w' of the leaf-springs has no effect whatsoever upon stress). However, in many applications such as that discussed here, neither of these two solutions is viable, either due to spatial constraints which make accommodating longer leaf-springs impossible, or due to the attendant degradation in spring

performance resulting from the reduction in thickness. In such cases, the only remaining alternative is to reduce stress by optimizing the shape of the leaf-springs, thus moving from a constant cross section to a variable cross section.

A review of the literature regarding the optimization of flexural pivots for stress reduction shows that the majority of work to date has focused on notch-based lumped-compliance hinges[7,8,9,10]. The potential for stress reduction through shape optimization as applied to distributed compliance leaf-type springs in crossed flexure pivots remains however to be investigated. This question constitutes precisely the object of study of the present paper. The methodology employed to tackle the analysis is covered in Section 2, while the findings are presented in Section 3. The main conclusions are outlined in Section 4.

2. METHODOLOGY

2.1 Leaf-spring crossed flexure pivots

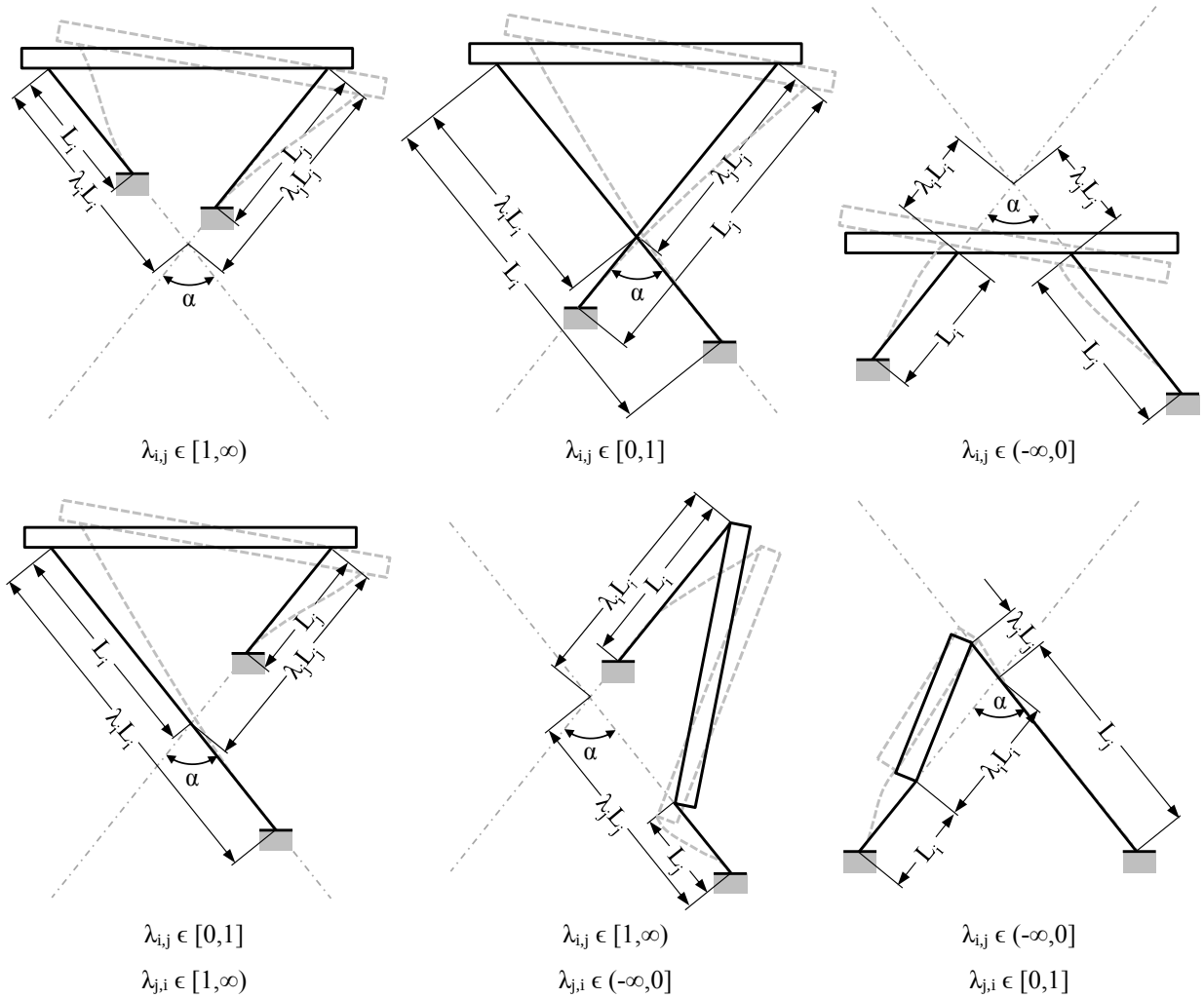

Figure 3. Different configurations of crossed flexure pivots based on the lambda parameter of their individual leaf-springs ($\lambda_{i,j}$).

Any crossed flexure pivot may be defined by three independent 'geometrical parameters' which determine its configuration: the angle 'α' between the oblique springs (see Fig. 3) and the point at which these cross (specified by parameters '$\lambda_{i,j}$'). The parameters associated with the dimensions of each leaf-spring (i.e. their individual lengths '$L_{i,j}$',

thicknesses '$t_{i,j}$' and widths '$w_{i,j}$') are referred to as 'shape parameters', simply to distinguish them from 'geometrical parameters'[11]. The 'λ' parameter of each leaf-spring is defined as the ratio of the distance between its moving end and the centre of rotation to its total length (see Fig. 3). Based on this parameter, crossed flexure pivots may be categorized into the six configurations shown in Fig. 3 which, contrary to what it may seem, are simply different embodiments of the same topology.

In theory, $\lambda_{j,i}$ may take any value in the range of $(-\infty, \infty)$. However, in practical applications $\lambda_{i,j}$ always lie within the range[6] of [-1, 2]. It is worth pointing out that two configurations with leaf-spring pairs of parameters $\lambda_{j,i}$ and $\lambda'_{j,i}=1-\lambda_{j,i}$ have the same geometry but opposite boundary conditions[12] (i.e. the fixed ends of the leaf-springs in one configuration become the moving ends in the other and vice versa). A single configuration therefore suffices to study the performance characteristics of both, as long as the analysis is carried out both from a fixed frame of reference (fixed end) and a relative frame of reference (moving end) perspective. This greatly facilitates the analysis of this type of flexural pivot, as the study of any performance characteristic can be performed only on half of the 'λ' range of interest (e.g. [0.5, 2]) and then extended to the other half (e.g. [-1, 0.5]) simply by carrying out the appropriate variable changes to account for the change in the frame of reference.

2.2 Stress analysis method

The optimization of a mechanical component usually involves the employment of finite element analysis (FEA) dependent methods, as this is generally the only tool capable of accurately predicting stress —or other mechanical characteristics— in a freely evolving geometry of random initial shape. In the case of standard (i.e. constant cross section) crossed flexure pivot leaf-springs, however, as they are slender prismatic elements of rectangular cross section, their mechanical behaviour can be accurately predicted simply through classic beam theory provided the deflection angle is kept small (i.e. $\theta_z \leq 15°$). Strictly speaking, classic beam theory is only applicable to slender prismatic elements (i.e. with a straight longitudinal axis and of constant cross section). However, as noted by Timoshenko[13], it also gives satisfactory results on variable cross section beams as long as they have a straight longitudinal axis and their cross sectional variation along their length is small (i.e. slope≤tan15°). The three-dimensional optimization of crossed flexure pivot leaf-springs happens to meet these conditions and is therefore compatible with classic beam theory. Indeed, for reasons explained in Section 2.3, the longitudinal axis of the resulting optimized leaf-springs will be straight (i.e. they will be symmetrical about the x-y and x-z planes as per Fig. 8). Furthermore, their cross section must also be of rectangular shape due to manufacturing constraints. On the other hand, standard crossed flexure pivot leaf-springs have length to thickness ratios in excess of L/t>25. Consequently, changes in thickness along their length will be smooth even in their optimized form, resulting in moderate slopes (dy/dx≤tan15°, as per Fig. 8) as the results shown in Section 3.1 demonstrate. As for the width to length ratios of standard crossed flexure pivot leaf-springs, these typically lie in the range $0.1<w/L<0.75$. In principle, the resulting optimized leaf-springs could exhibit large variations in width, therefore precluding the applicability of classic beam theory. However, if the width-wise compactness is to be retained in the resulting optimized profiles, dz/dx will have to be constrained in order to avoid unpractical, excessively large w_{max}/w_{min} ratios (see Figs. 8 and 9). Therefore, assuming the reference optimized profiles to have a $w_{min}/L=0.1$ (i.e. the practical minimum), if dz/dx≤tan15° it is possible to ensure that w_{max}/w_{min} stays within reasonable limits ($w_{max}/w_{min} \leq 6.4=(0.1L+2L\tan 15°)/(0.1*L)$, i.e. $w_{max}/L \leq 0.64$), leaving, furthermore, some room for scaling up of the optimum profile to higher w_{min}/L ratios. As shown later in Section 3.1, this constraint set upon dz/dx barely affects the achievable stress reduction (about 2% less than width-wise unconstrained profiles), while yielding acceptable w_{max}/w_{min} ratios. These reasons outlined above —which are validated by the results presented in Section 3.1— allow the stress analysis to be performed through a linear strain energy formulation (derived from Castigliano's first theorem) in lieu of the finite element method. The advantage of this approach is not so much the simplicity gained, but the fact that analytical formulation offers much greater insight into the factors governing the optimization problem than the finite element method, whose numerical nature makes drawing general conclusions difficult.

In any crossed flexure pivot configuration, the moving ends of the leaf-springs need to satisfy a series of deformation compatibility relationships (see Fig. 4), regardless of whether the leaf-springs are of constant or variable cross section. For small deflection angles (i.e. $|\theta_z| \leq 15°$), it is common practice[6,11,12,14-20] to take said deformation compatibility equations as:

$$u_{y_i} = \lambda_i L_i \theta_z \quad (1)$$

$$u_{y_j} = \lambda_j L_j \theta_z \quad (2)$$

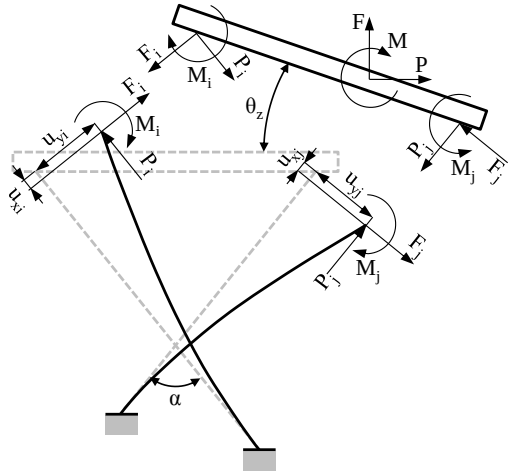

Figure 4. Displacements and reaction at the moving ends of the leaf-springs of a crossed flexure pivot subjected to general planar loading state.

where the underlying assumptions are $u_{xi}=u_{xj}\approx 0$ (as $u_{xi}<<u_{yi}$ and $u_{xi}<<u_{yi}$) and $\sin\theta_z\approx\theta_z$ and $\cos\theta_z\approx 1$. Accordingly, the deflections at the moving end of each leaf-spring can be expressed as functions of the rotational angle of the pivot (θ_z) as shown in Eq. 3:

$$\{u\}=\begin{Bmatrix} u_x \\ u_y \\ \theta_z \end{Bmatrix}=\begin{Bmatrix} 0 \\ \lambda L\theta_z \\ \theta_z \end{Bmatrix} \tag{3}$$

This constitutes an important result as it allows the leaf-springs to be studied as isolated individual entities, susceptible of being modelled as shown in Fig. 5:

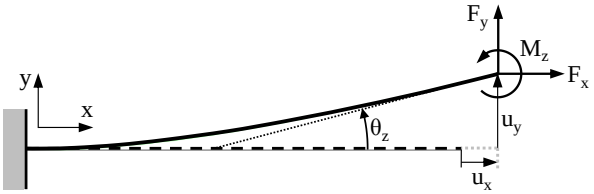

Figure 5. Schematic of a 2D cantilever beam subjected to a general loading case. The encastre (left) and free (right) ends represent the leaf-spring's fixed and moving ends respectively.

In order to determine the stress field of the leaf-springs, it is first necessary to calculate the vector of loads {L} acting at their moving end. This can be calculated through Eq. 4:

$$\{L\}=[K]\{u\}=[C]^{-1}\{u\}=\begin{bmatrix} C_{x\text{-}F_x} & 0 & 0 \\ 0 & C_{y\text{-}F_y} & C_{y\text{-}M_z} \\ 0 & C_{\theta_z\text{-}F_y} & C_{\theta_z\text{-}M_z} \end{bmatrix}^{-1}\begin{Bmatrix} 0 \\ \lambda L\theta_z \\ \theta_z \end{Bmatrix}=\begin{Bmatrix} F_x \\ F_y \\ M_z \end{Bmatrix} \tag{4}$$

where [C] is the compliance matrix, which is symmetrical and solely dependent on the geometry and material of the leaf-spring. The compliances within [C] can be calculated as explained by Lobontiu[21] (see Eqs. 6-9).

Bearing in mind that the shear stresses in the leaf-springs are negligible due to their slenderness ($L/t_{min}>25$), the only significant stress will be that arising from bending[6,11]. Therefore, the maximum stress at any one cross-section can be calculated simply by applying Navier's formula:

$$\sigma_{max}(x)=\frac{M_z(x)\cdot y(x)}{I_z(x)}=\frac{\left(M_z+x\cdot F_y\right)\cdot y(x)}{I_z(x)} \quad \forall\, x\in[0,L] \tag{5}$$

It is important to point out that Eq. 5 provides satisfactory stress results at any point along a leaf-spring except at its ends (i.e. the points of connection to the fixed and moving stages of the pivot), where stress concentration might exist. For the

purposes of this study, however, stress concentration need not be explicitly taken into account due primarily to two reasons: firstly, because both the constant cross section and the optimized leaf-springs are equally affected by this phenomenon; and secondly, because whether stress concentration does exist, and if so, how significant this is, is largely dependent on the method employed to attach the leaf-springs to the fixed and moving stages of the pivot (see Fig. 6). In any case, if it does exist, the effect of a stress raiser can always be modelled as a factor K_t that amplifies the nominal stress σ_{nom} at the root, such that the true stress equals $K_t \cdot \sigma_{nom}$. The value of said K_t is not dictated by the thickness and width profiles of the leaf-spring, but by factors dependent on the specific method employed to attach the leaf-spring to the end blocks, such as: the presence or absence of a fillet at the root and its specific geometry, the mechanical properties of the adhesive employed and the thickness and geometry of the glue line, potential residual stresses generated within the heat affected zone of the weld, etc. Consequently, the stress concentration can always be considered and addressed as a separate problem, independently of the specific shape of the leaf-spring's thickness and width profiles and its associated nominal stress at the root. On these grounds, in this work the predicted relative stress between the optimized and the constant cross section leaf-springs is quantified directly as the quotient of their respective maximum nominal stresses (see Eq. 20).

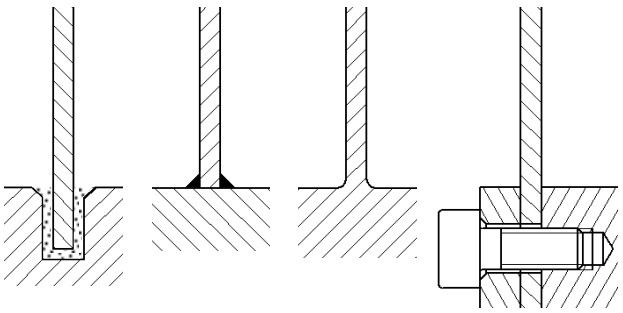

Figure 6. Possible methods of attaching the ends of the leaf-springs to the fixed and moving stages of the pivot: (a) glued within a slit; (b) brazed/welded; (c) monolithic construction; (d) bolted/clamped.

Nevertheless, the FE validation presented in Section 3.1 does implicitly account for stress concentration, since a tangent fillet of the same radius was added either end of both the optimized and the constant cross section leaf-springs in all the FE models employed. Consequently, the fact that the FE results are in good agreement with the predictions (as later shown in Section 3.1) goes to show that it is indeed acceptable to quantify the relative stress reduction between the optimized and the constant cross section leaf-springs directly as the quotient of their respective maximum nominal stresses.

2.3 Definition of the thickness and width profiles

In order to find the absolute optimum shape of a leaf-spring, its cross section should be allowed to freely vary along its longitudinal axis. However, a completely freely varying cross section could lead to an optimized profile shape impossible to manufacture and therefore of no practical use. Due to their distributed compliance nature, crossed flexure pivot leaf-springs are, even in their optimized form, necessarily very slender mechanical members ($L/t_{min}>25$). This implies that their optimized thickness profiles will exhibit a smooth variation (i.e. $dy/dx<\tan 15°$) and that their average thicknesses will be much smaller than their lengths. From all the existing manufacturing processes, the only two capable of accurately generating such thin and smoothly varying metallic profiles are —depending on the absolute dimensions of the leaf-springs—wire electrical discharge machining (WEDM) and X-ray LIGA, a manufacturing process which offers some impressive capabilities such as[22,23]: applicability to a wide variety of materials including most metals, high aspect ratios (height/depth) in excess of 100:1, parallel side walls with a flank angle of the order of 89.95°, smooth side walls with Ra = 10 nm, structural heights from tens of μm up to 1cm, as well as structural details of the order of 0.2μm, with a tolerance of 0.3μm over distances of cm. However, both WEDM and X-ray LIGA produce prismatic parts (i.e. straight extrusions of two-dimensional profiles), meaning that the thickness of the leaf-springs can only be made to vary along the longitudinal axis of the leaf-spring, while having to keep it constant along the width-wise direction (i.e. z axis in Fig. 7). The optimized width profile can subsequently be WEDM-ed, after turning the leaf-springs 90° about their longitudinal axis. As a consequence of this manufacturing sequence, the cross section of the optimized leaf-springs will necessarily have to be rectangular.

On the other hand, if the optimized leaf-springs are to perform equally at positive and negative angles of rotation (θ_z), they must be symmetrical about their longitudinal axis (i.e. x-z plane in Fig. 7). Furthermore, to avoid the appearance of unwanted out-of-plane moments when loading the pivot about its centre, the leaf-springs will also have to be symmetrical about the x-y plane. Based on this double symmetry, the thickness and width profiles can be written as 't(x)=2y(x)' and 'w(x)=2z(x)', where 'y(x)' and 'z(x)' can each be defined through a piecewise polynomial (see Fig. 7) passing through 'n' evenly spaced interpolation points. The entire optimized shape is thus defined through '2n' variables: namely, the 'y' and 'z' coordinates of each of the 'n' evenly spaced interpolation points. Said 'y(x)' and 'z(x)' polynomials can be obtained by employing the piecewise cubic Hermite interpolation package (PCHIP)[24,25], which yields smoother curves than most other methods including traditional piecewise cubic spline interpolation. Naturally, the higher the number 'n' of interpolation points, the larger and more varied the mathematical space of solutions (in terms of possible profiles) and consequently, the potential reduction in maximum stress. However, as 'n' grows, so does the size and complexity of the polynomials defining the thickness and width profiles, as well as the computational time required to carry out the optimization. Thus, there is bound to be an 'optimum' number of interpolation points 'n' that yields the best compromise between size/complexity of the polynomials defining the optimized profiles and achieved stress reduction. Section 3.1 discusses how this number 'n' is determined.

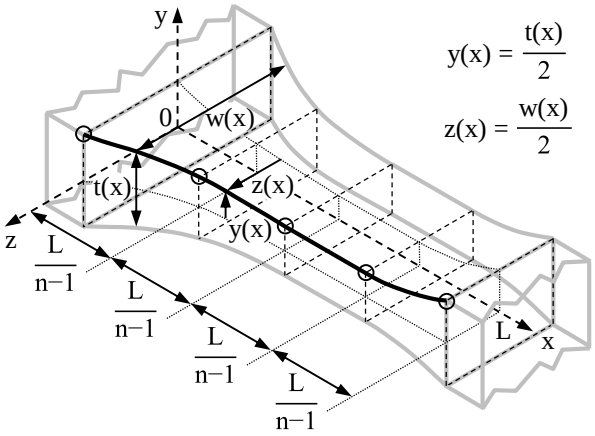

Figure 7. Thickness t(x) and width w(x) profiles defined by 'n' evenly spaced interpolation points.

2.4 Analysis of the influence of the design parameters on maximum stress

Before designing the optimization procedure to be employed, it is important to analyse both the influence of the different design parameters on maximum stress and how this scales with leaf-spring size. To this end, let us assume that for a given reference leaf-spring of length 'L_1', thickness 't_{min1}' and width 'w_{min1}' the optimum profiles 't(x)' and 'w(x)' are known (see thickness and width profiles on the left hand side of Fig. 8). For these profiles —which will be referred to as the 'reference profiles'—, the compliance coefficients in Eq. 4 can be written as:

$$C_{x\text{-}F_x}\big|_{L_1} = \frac{1}{E}\int_0^{L_1} \frac{dx}{w(x)t(x)} = \frac{1}{E}\cdot S_{x\text{-}F_x}\big|_{L_1} \tag{6}$$

$$C_{y\text{-}F_y}\big|_{L_1} = \frac{12}{E}\int_0^{L_1} \frac{x^2 dx}{w(x)[t(x)]^3} = \frac{12}{E}\cdot S_{y\text{-}F_y}\big|_{L_1} \tag{7}$$

$$C_{y\text{-}M_z}\big|_{L_1} = C_{\theta_z\text{-}F_y}\big|_{L_1} = \frac{12}{E}\int_0^{L_1} \frac{x\,dx}{w(x)[t(x)]^3} = \frac{12}{E}\cdot S_{y\text{-}M_z}\big|_{L_1} \tag{8}$$

$$C_{\theta_z\text{-}M_z}\big|_{L_1} = \frac{12}{E}\int_0^{L_1} \frac{dx}{w(x)[t(x)]^3} = \frac{12}{E}\cdot S_{\theta_z\text{-}M_z}\big|_{L_1} \tag{9}$$

Consider now a second leaf-spring resulting from linearly scaling the reference profiles from 'L_1' to 'L_2' , from 't_{min1}' to 't_{min2}' and from 'w_{min1}' to 'w_{min2}' (see thickness and width profiles on the right hand side of Fig. 8). For this second set of profiles —which will be referred to as the 'scaled profiles'—the compliance coefficients will be:

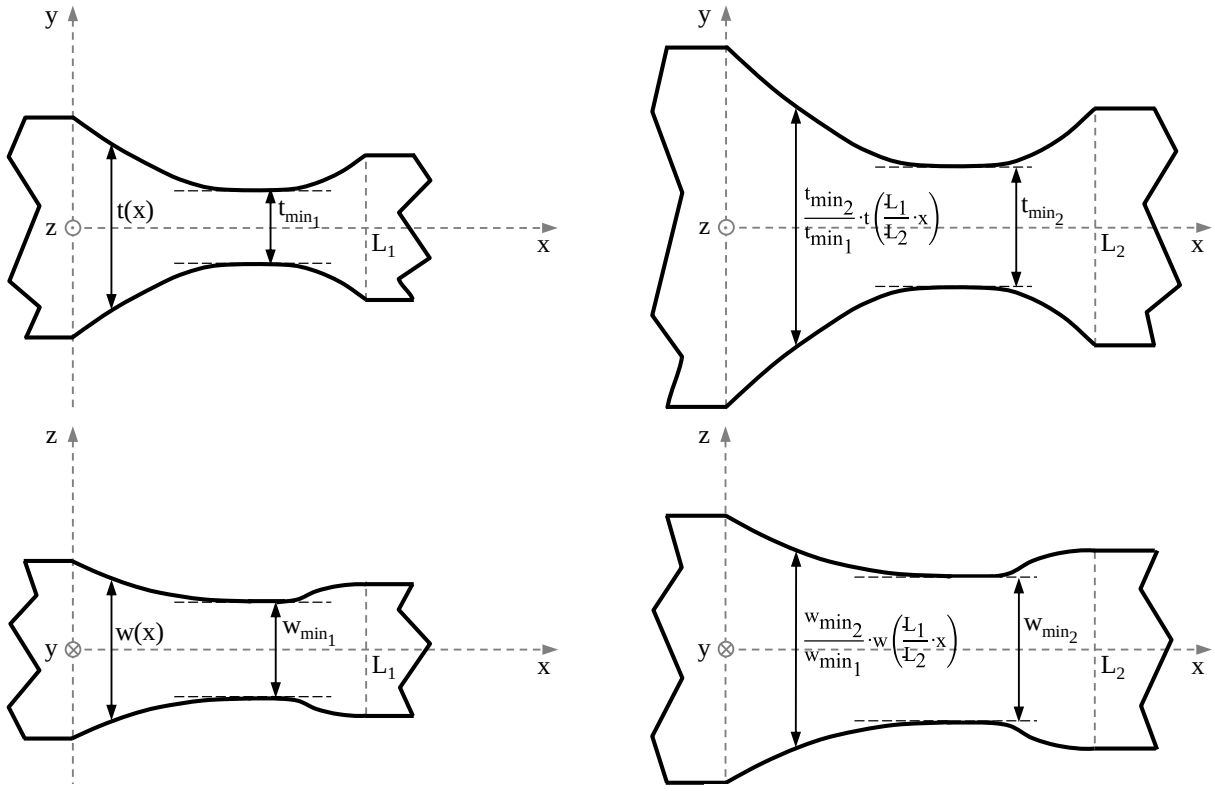

Figure 8. Top Left: reference variable thickness profile; Top right: linearly scaled version of the reference thickness profile; Bottom Left: reference variable width profile; Bottom right: linearly scaled version of the reference width profile.

$$C_{x\text{-}F_x}\big|_{L_2} = \frac{1}{E}\int_0^{L_2} \frac{f_w f_t dx}{w(f_L x)t(f_L x)} = \frac{1}{E}\int_0^{L_1} \frac{f_w f_t dz}{f_L w(z)t(z)} = \frac{1}{E}\cdot\frac{f_w f_t}{f_L}\cdot S_{x\text{-}F_x}\big|_{L_1} \quad (10)$$

$$C_{y\text{-}F_y}\big|_{L_2} = \frac{12}{E}\int_0^{L_2} \frac{f_w f_t^3 x^2 dx}{w(f_L x)[t(f_L x)]^3} = \frac{12}{E}\int_0^{L_1} \frac{f_w f_t^3 z^2 dz}{f_L^3 w(z)[t(z)]^3} = \frac{12}{E}\cdot\frac{f_w f_t^3}{f_L^3}\cdot S_{y\text{-}F_y}\big|_{L_1} \quad (11)$$

$$C_{y\text{-}M_z}\big|_{L_2} = C_{\theta_z\text{-}F_y}\big|_{L_2} = \frac{12}{E}\int_0^{L_2} \frac{f_w f_t^3 x\, dx}{w(f_L x)[t(f_L x)]^3} = \frac{12}{E}\int_0^{L_1} \frac{f_w f_t^3 z\, dz}{f_L^2 w(z)[t(z)]^3} = \frac{12}{E}\cdot\frac{f_w f_t^3}{f_L^2}\cdot S_{y\text{-}M_z}\big|_{L_1} \quad (12)$$

$$C_{\theta_z\text{-}M_z}\big|_{L_2} = \frac{12}{E}\int_0^{L_2} \frac{f_w f_t^3 dx}{w(f_L x)[t(f_L x)]^3} = \frac{12}{E}\int_0^{L_1} \frac{f_w f_t^3 dz}{f_L w(z)[t(z)]^3} = \frac{12}{E}\cdot\frac{f_w f_t^3}{f_L}\cdot S_{\theta_z\text{-}M_z}\big|_{L_1} \quad (13)$$

where $f_L = L_1/L_2$, $f_t = t_{min1}/t_{min2}$ and $f_w = w_{min1}/w_{min2}$. It is also noteworthy that applying the variable change '$z = f_L \cdot x$' in Eqs. 10-13 enables the integrals for the scaled profiles to be expressed in terms of those of the reference profiles. Once the compliance coefficients are known, the forces acting at the free end of the scaled profile can be calculated according to Eq. 4:

$$F_y\big|_{L_2} = \frac{E\theta_z}{12}\cdot\frac{f_L^2}{f_w f_t^3}\cdot\left(\frac{\lambda L_1 S_{\theta_z\text{-}M_z}\big|_{L_1} - S_{y\text{-}M_z}\big|_{L_1}}{S_{y\text{-}F_y}\big|_{L_1} S_{\theta_z\text{-}M_z}\big|_{L_1} - S_{y\text{-}M_z}\big|_{L_1}^2}\right) \quad (14)$$

$$M_z\big|_{L_2} = \frac{E\theta_z}{12}\cdot\frac{f_L}{f_w f_t^3}\cdot\left(\frac{-\lambda L_1 S_{y\text{-}M_z}\big|_{L_1} + S_{y\text{-}F_y}\big|_{L_1}}{S_{y\text{-}F_y}\big|_{L_1} S_{\theta_z\text{-}M_z}\big|_{L_1} - S_{y\text{-}M_z}\big|_{L_1}^2}\right) \quad (15)$$

Accordingly, the bending moment along the scaled profile will be:

$$M_z(x)|_{L_2}=x\cdot F_y\Big|_{L_2}+M_z|_{L_2}=\frac{E\theta_z}{12}\cdot\frac{f_L}{f_w f_t^3}\cdot\left(\frac{-\lambda L_1 S_{y\text{-}M_z}\Big|_{L_1}+S_{y\text{-}F_y}\Big|_{L_1}+f_L x\left(\lambda L_1 S_{\theta_z\text{-}M_z}\Big|_{L_1}-S_{y\text{-}M_z}\Big|_{L_1}\right)}{S_{y\text{-}F_y}\Big|_{L_1}S_{\theta_z\text{-}M_z}\Big|_{L_1}-S_{y\text{-}M_z}\Big|_{L_1}^{\,2}}\right) \quad (16)$$

Taking this result into Eq. 5, the maximum stress at any cross-section along the scaled profile will be:

$$\sigma_{max}(x)|_{L_2}=\frac{M_z(x)|_{L_2}\cdot\frac{t(f_L x)}{2}}{I_z(f_L x)}=$$

$$=\frac{f_L}{f_t}\cdot\frac{E\theta_z}{2}\cdot\left\{\frac{-\lambda L_1 S_{y\text{-}M_z}\Big|_{L_1}+S_{y\text{-}F_y}\Big|_{L_1}+f_L x\left(\lambda L_1 S_{\theta_z\text{-}M_z}\Big|_{L_1}-S_{y\text{-}M_z}\Big|_{L_1}\right)}{w(f_L x)\left[t(f_L x)\right]^2\left(S_{y\text{-}F_y}\Big|_{L_1}S_{\theta_z\text{-}M_z}\Big|_{L_1}-S_{y\text{-}M_z}\Big|_{L_1}^{\,2}\right)}\right\}\ \forall\, x\in[0,L_2] \quad (17)$$

Eqs. 17 constitutes a very important result as they provide an invaluable insight into the parameters that affect the maximum stress and its distribution along the leaf-spring. Both equations have two distinctive parts: an expression between curly brackets — which determines the shape of the maximum stress distribution along the length of the leaf-spring— and a series of preceding coefficients which simply modulate its absolute value. As Eqs. 17 shows, the expression between curly brackets depends solely on terms belonging to the reference leaf-spring, regardless of the absolute dimensions of the scaled leaf-spring —note that the term '$(L_1/L_2)x$' for $x \in [0, L_2]$ is equivalent to just 'x' for $x \in [0, L_1]$. Consequently, if the optimum thickness 't(x)' and width 'w(x)' profiles for a reference leaf-spring of dimensions 'L_1', 't_{min1}' and 'w_{min1}' are known, the optimum thickness and width profiles for any other scaled leaf-spring of dimensions 'L_2', 't_{min2}' and 'w_{min2}' will also automatically be known, being simply the result of linearly scaling the optimum thickness and width profiles for the reference leaf-spring 't(x)'and 'w(x)'. Thus, it can be concluded that the relative shapes of the optimum profiles will depend only on the specific 'λ' parameter of the leaf-spring in question, and that they will be independent of the material (i.e. E) and the angle of rotation (i.e. θ_z).

Another conclusion of interest is that the absolute stress levels in the optimized leaf-springs are dependent on their absolute length 'L' (through 'f_L') and thickness 't_{min}' (through 'f_t') dimensions, but independent of their absolute width 'w_{min}' (note the absence of 'f_w' in Eq. 17). Therefore, for a given 'λ', two optimized leafs-springs of the same length 'L' and minimum thickness 't_{min}' but different minimum widths 'w_{min1}' and 'w_{min2}' will still be subjected to the same maximum stress. Consequently, the minimum width of the optimized width profiles 'w_{min}' remains a 'free' variable with no effect upon maximum stress, which can be used to satisfy other performance requirements in terms of rotational stiffness, natural frequencies, etc. or to minimize the effects on stress of out-of-plane loading if present.

2.5 Description of the optimization procedure

The conclusions drawn in Section 2.4 are of great importance for the design of the optimization procedure, which for the purposes of this paper was programmed on Matlab[26]. The definition of the thickness and width profiles and the determination of the maximum stress in each iteration were carried out as described earlier in this section. With regard to the optimization algorithm employed, three different types already built into the aforementioned software were trialled: patternsearch, genetic algorithm (ga) and particle swarm optimization (pso). The reason for employing three different algorithms was two-fold: first, to validate the individual results by cross-checking, thus avoiding possible local optima; and second, to achieve as accurate (and hence as optimum) a solution as possible, since each algorithm yields a slightly different answer even under the same stopping/convergence criteria. For the reasons explained in Section 2.1, the optimization was carried out for a selection of 'λ' parameters covering the range [0.5, 2]. Furthermore, in order to investigate the effect of 'n' (number of interpolation points used for the definition of the thickness profile) on the achievable stress reduction, for each 'λ' case analysed, six different numbers of interpolation points were utilized to define the thickness profile, namely: n = 2, 3, 5, 9, 17 and 33. Also, for practical reasons all optimization cases were carried out on a reference leaf-spring of dimensions 'L_1', 't_{min1}' and 'w_{min1}' equal to unity. This way, the resulting optimized thickness 't(x)' and width 'w(x)'profiles can be easily scaled to any other leaf-spring of dimensions 'L_2', 't_{min2}' and 'w_{min2}' simply by multiplying 't(x)' by 't_{min2}', 'w(x)' by 'w_{min2}' and by substituting 'x', for 'L_2x' (see Fig. 8). Furthermore, Young's

modulus (E), the angle of rotation (θ_z) and the horizontal displacement of the moving stage (δ_y) were also taken as equal to unity, as they have no influence on the resulting optimized profiles. As for the optimization constraints, only two conditions were imposed upon the algorithm. Firstly, for the slope at any point throughout the optimized thickness and width profiles to be $dy/dx \leq 25 \cdot \tan 15°$ and $dz/dx \leq 10 \cdot \tan 15°$ respectively, as defined in Fig. 7 (note that the leaf-springs will always have a minimum slenderness ratio of $L/t_{min}=25$ and $w_{min}/L=0.1$). Secondly, for the thickness and width at any one point along the optimized leaf-springs to be equal or greater than that of their constant cross section counterparts, i.e. $t(x) \geq t_{min1}=1 \wedge w(x) \geq w_{min1}=1 \; \forall \; x \in [0, L]$ (an unconstrained thickness and/or width could result in local points of zero thickness, which is physically meaningless as any leaf-spring must have physical continuity between its ends). An important direct consequence of this second constraint is that crossed flexure pivots with optimized leaf-springs will necessarily have an improved instability/buckling behaviour compared to those with constant cross section leaf-springs.

2.6 Parametrical dependence analysis of the target result quantities

Equally important to defining an appropriate optimization strategy is to establish the most valuable and meaningful results that should be obtained from the analysis and the most appropriate way to present these. As a rule, results should be presented in a way as general as possible, ideally in a non-dimensional form. In this case, since the objective of the study is an optimization for the reduction of maximum stress, the key result to present will be the reduction in maximum stress achieved with the optimized leaf-springs, relative to their corresponding constant cross section counterparts. In order to determine the best way to present this non-dimensional quantity, it is important to identify the parameters it depends on.

The maximum stress for a constant cross section leaf-spring of dimensions 'L_2', 't_{min2}' and 'w_{min2}' can be written as[6]:

$$\sigma_{max}|_{const,\,L_2} = \frac{(3\lambda\text{-}1) E t_{min_2} \theta_z}{L_2} \tag{18}$$

Similarly, according to Eq. 17 the maximum stress for the corresponding optimized variable cross section leaf-spring of dimensions 'L_2', 't_{min2}' and 'w_{min2}' can be written as:

$$\sigma_{max}\left(x_{\sigma_{max}}\right)\Big|_{optim,\,L_2} = \frac{f_L}{f_t} \cdot \frac{E\theta_z}{2} \cdot \left\{ \frac{-\lambda L_1 S_{y\text{-}M_z}\Big|_{L_1} + S_{y\text{-}F_y}\Big|_{L_1} + f_L x_{\sigma_{max}} \left(\lambda L_1 S_{\theta_z\text{-}M_z}\Big|_{L_1} - S_{y\text{-}M_z}\Big|_{L_1} \right)}{w\left(f_L x_{\sigma_{max}}\right)\left[t\left(f_L x_{\sigma_{max}}\right)\right]^2 \left(S_{y\text{-}F_y}\Big|_{L_1} S_{\theta_z\text{-}M_z}\Big|_{L_1} - S_{y\text{-}M_z}\Big|_{L_1}{}^2 \right)} \right\} \tag{19}$$

where '$x_{\sigma_{max}}$' represents the 'x' coordinate of the cross section at which the absolute maximum stress in the leaf-spring occurs. It should be noted that the maximum stress in Eq. 19 is written in terms of a reference optimized leaf-spring of dimensions 'L_1', 't_{min1}' and 'w_{min1}'. The relative reduction in stress can consequently be calculated by dividing Eq. 19 by Eq. 18:

$$\frac{\sigma_{max}\left(x_{\sigma_{max}}\right)\Big|_{L_2}\Big|_{optim,\,L_2}}{\sigma_{max}|_{const,\,L_2}} = \frac{L_1}{2t_{min_1}} \cdot \left\{ \frac{-\lambda L_1 S_{y\text{-}M_z}\Big|_{L_1} + S_{y\text{-}F_y}\Big|_{L_1} + f_L x_{\sigma_{max}} \left(\lambda L_1 S_{\theta_z\text{-}M_z}\Big|_{L_1} - S_{y\text{-}M_z}\Big|_{L_1} \right)}{(3\lambda\text{-}1) w\left(f_L x_{\sigma_{max}}\right)\left[t\left(f_L x_{\sigma_{max}}\right)\right]^2 \left(S_{y\text{-}F_y}\Big|_{L_1} S_{\theta_z\text{-}M_z}\Big|_{L_1} - S_{y\text{-}M_z}\Big|_{L_1}{}^2 \right)} \right\} = f(\lambda) \tag{20}$$

Since Eq. 20 shows no dependency on any of the dimensions of the profiles compared (i.e. 'L_2', 't_{min2}' or 'w_{min2}'), it can be concluded that the relative reduction in maximum stress is a function which depends solely upon the 'λ' parameter of the leaf-springs in question.

3. RESULTS

3.1 Optimized leaf-springs and achieved reduction in maximum stress

As predicted in the previous section, the number of interpolation points used to define the optimized leaf-springs does indeed have an impact on the achievable stress reduction. This can be observed in Fig. 9, which shows a three-dimensional plot of the predicted stress reduction as per Eq. 20, on the domain "number of interpolation points 'n' vs. 'λ' parameter". In said plot, as 'n' increases beyond n=2 —which is the smallest number of evenly spaced interpolation points with which a variable cross section profile can be defined, that is, one interpolation point at each end of the leaf-spring, therefore

resulting in a constant taper profile—, the relative maximum stress can be seen to rapidly decrease in a hyperbolic-like manner until it eventually becomes almost asymptotic. As noted in Section 2.3, the ideal 'n' will be that which yields the best compromise between size/complexity of the polynomials defining the optimized profiles and achieved stress reduction. According to Fig. 9, increasing 'n' beyond n=17 yields virtually no further reduction in stress (the reduction in relative maximum stress between n=17 and n=33 is less than 0.5% for all 'λ'). Therefore, it can be concluded that 17 (or close to 17) is probably the most suitable number of evenly spaced interpolation points to define the optimum thickness and width profiles of the leaf-springs.

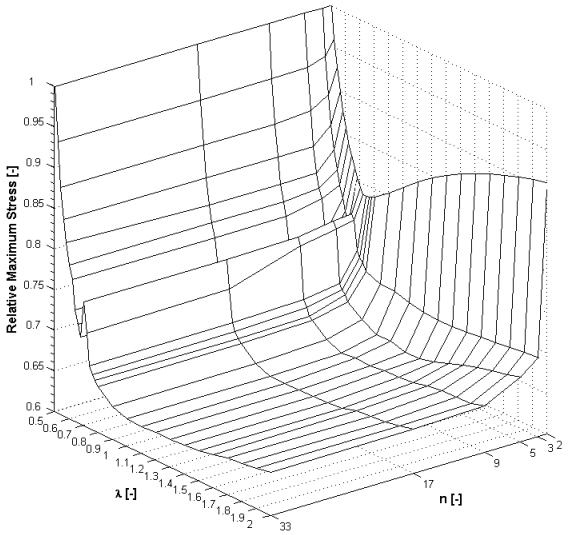

Figure 9. Plots showing predicted relative maximum stress as per Eq. 20 vs. number of interpolation points 'n', for $\lambda \in [0.5, 2]$.

Having concluded that, irrespective of the 'λ' parameter, 17 evenly spaced interpolation points offer the best compromise between size/complexity of the polynomials defining the optimized profiles and achieved stress reduction, the results that follow refer to the optimized profiles as defined by n=17. These optimized profiles are plotted in Fig. 10. Their exact numerical definition is given in non-dimensional form in Table 1 to allow easy scalability to leaf-springs of any length 'L', minimum thickness 't_{min}' and width 'w_{min}' (as explained in Section 2.4). It is important to bear in mind that for $\lambda \in [0.5, 2]$ the coordinate 'x/L=0' in Fig. 10 and Table 1 refers to the 'fixed end' of the leaf springs. Conversely, for $\lambda \in [-1, 0.5]$ the coordinate 'x/L=0' in Fig. 10 and Table 1 would refer to the 'moving end' of the leaf springs, in accordance with the explanation given in Section 2.1. Fig. 11 shows what the optimized leaf-springs would like in the specific case of the AGF mechanism's crossed flexure pivots.

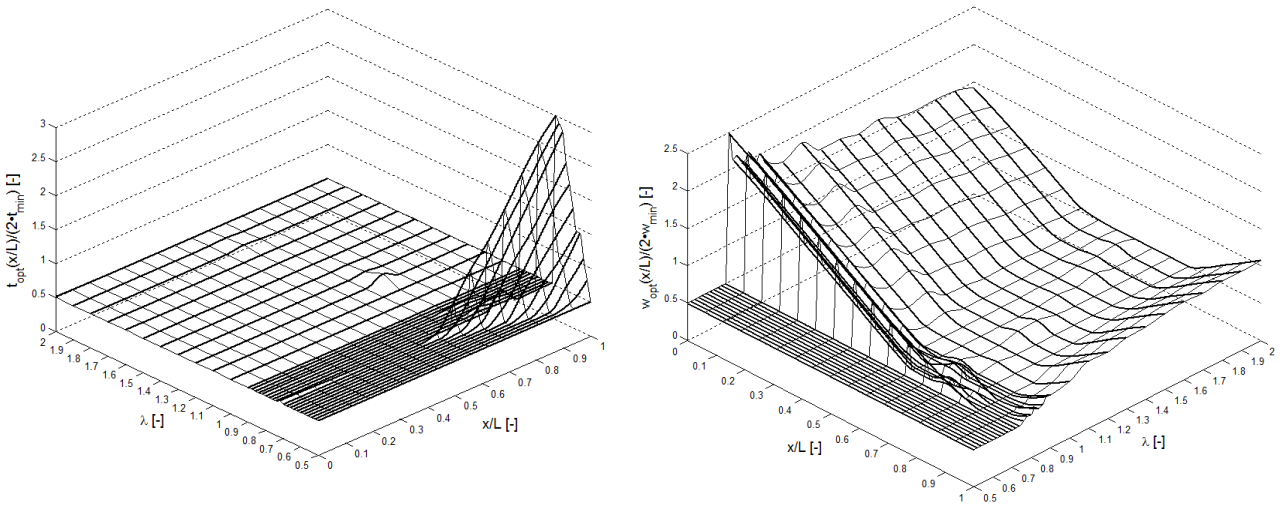

Figure 10. Plot showing the optimum thickness (left) and width (right) profiles in non-dimensional form, on the domain "non-dimensional leaf-spring length vs. 'λ' parameter".

An important conclusion that can be drawn by looking at Fig. 10 is that, for $\lambda \in [0.5, 0.7]$, the optimum leaf-spring shapes yielding lowest stress may be obtained simply by optimizing the thickness profile of the leaf-springs while keeping their width constant (see Table 1). Conversely, for $\lambda>0.7$ it is the width that seems to be the key dimension providing the reduction in stress, as the thickness of the optimized profiles remains almost constant. Although as shown in Table 1 the thickness for this latter range of 'λ' is not strictly constant, its variation is so small that it is suspected that virtually the same stress reductions would have been obtained had the thickness been kept absolutely constant. Consequently, it can be concluded that for $\lambda>0.7$ the optimum leaf-spring shape yielding lowest stress could in all probability be obtained simply by optimizing the width profile of the leaf-springs while keeping the thickness constant. This latter finding is of great practical transcendence: firstly, because varying the width of a leaf-spring is, from a manufacturing perspective, much easier than varying its thickness; and secondly, because of the many complex flexures based on crossed flexure pivots of $\lambda>0.7$ that could benefit from this such as the cartwheel hinge[27], the 'butterfly' flexure pivot[28], the compound generalized cross-spring pivot[12,29], the anti-symmetric double leaf-type isosceles-trapezoidal flexure (ADLIF)[30], etc.

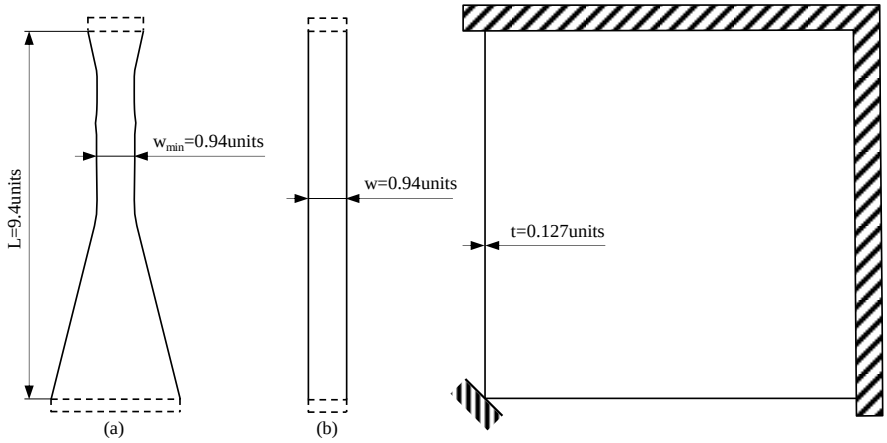

Figure 11. Optimized (a) and constant cross section (b) leaf-springs for AGF mechanism's crossed flexure pivots ($\lambda \approx 1$).

Fig. 12 shows the predicted stress reduction for the three-dimensionally optimized leaf-springs as per Eq. 20. In order to test the validity of the assumptions regarding the maximum slope made in Section 2.2, a second set of optimizations was also performed for each of the 'λ' cases analysed eliminating the slope constraints. As observed in Fig. 12, both the constrained and unconstrained three-dimensional optimizations predict very similar stress reductions, with a negligible difference between them of around 2% on average. Although the geometrical definition of the unconstrained optimized profiles is not provided in the present publication, these were found to naturally present a thickness profile such that $dy/dx \leq \tan 15°$. Their width profile, however, clearly surpassed the $dz/dx \leq \tan 15°$ condition leading to $(w_{max}/w_{min})|_{uncon} >> (w_{max}/w_{min})|_{con}$, i.e. much wider profiles than those resulting from the constrained optimization. These two considerations, added to the fact that the stress reduction capability of the unconstrained optimized leaf-springs deteriorates with 'θ_z' quicker than that of their constrained counterparts —as the FEA results discussed later show—, indicate that unconstrained optimization actually yields worse results, thus justifying the slope assumptions made in Section 2.2.

In order to validate the predicted results, the stress reduction benefits of the optimized profiles were verified using Abaqus, a finite element analysis (FEA) software. To this end, two symmetrical crossed flexure pivot models were built for each 'λ' case analysed: one using leaf-springs of constant cross section and another using leaf-springs with the corresponding optimized shape. In all cases the leaf-springs were placed at 90° relative to each other (which is a standard value for 'α'[19,31]). Their dimensions were taken as L=9.4units, w_{min}=0.94units and t_{min}=0.127units (i.e. L/t_{min}=74 and w_{min}/L=0.1), and a tangent fillet of radius R=0.28units was added either end of both the optimized and the constant thickness leaf-springs (in the x-y plane) in all the FE models analysed. The leaf-springs were meshed using quadratic fully integrated three-dimensional hexahedral continuum elements —with a mesh density of a minimum of five elements across the thickness and a minimum of eighteen elements across the width—, to which a linearly elastic isotropic material with a Poisson's ratio of ν=0.3 and a Young's modulus of E=200GPa was assigned. The loading applied to the pivot in order to achieve the desired rotational deflection was a pure moment, and a non-linear type of analysis was performed. The relative maximum stress from the FEA was calculated as the quotient between the maximum von Mises equivalent stress of the optimized profiles and that of their corresponding constant cross section counterparts. The specific values used for the slenderness ratio 'L/t_{min}', 'w_{min}/L', the angle 'α' between the leaf-springs, the type of loading applied, etc. were selected to be representative of standard crossed flexure pivots. However, it should be noted that said values do have an effect on the specific results obtained, even if this effect would be small according to the analysis presented

in Section 2.4. Consequently, care should be exercised when extrapolating these FEA results to crossed flexure pivots subjected to a different loading regime and with other geometrical and/or shape parameters.

Table 1. Non-dimensional numerical definition of the optimum profiles for the set of different 'λ' parameters analysed.

		x/L [-]																
		0	**1/16**	**2/16**	**3/16**	**4/16**	**5/16**	**6/16**	**7/16**	**8/16**	**9/16**	**10/16**	**11/16**	**12/16**	**13/16**	**14/16**	**15/16**	**1**
$t_{opt}(x/L)/(2t_{min})$ [-]	**λ=0.50**	0.500000	0.500000	0.500000	0.500000	0.500000	0.500000	0.500000	0.500000	0.500000	0.500000	0.500000	0.500000	0.500000	0.500000	0.500000	0.500000	0.500000
	λ=0.52	0.500005	0.500004	0.500004	0.500003	0.500003	0.500006	0.500003	0.500002	0.500237	0.500001	0.500000	0.500000	0.500000	0.500003	0.500141	0.563596	0.794012
	λ=0.54	0.500011	0.500012	0.500008	0.500009	0.500007	0.500004	0.500006	0.500015	0.500002	0.500001	0.500000	0.500028	0.500000	0.500000	0.514198	0.788583	1.083115
	λ=0.56	0.500011	0.500007	0.500002	0.500001	0.500003	0.500000	0.500004	0.500000	0.500000	0.500000	0.500000	0.500000	0.500000	0.500397	0.663473	1.033386	1.435907
	λ=0.58	0.500163	0.500113	0.500064	0.500018	0.500000	0.500000	0.500000	0.500198	0.500000	0.500359	0.500000	0.500000	0.500000	0.591204	0.883966	1.129364	1.436857
	λ=0.60	0.500009	0.500000	0.500013	0.500000	0.500000	0.500000	0.500000	0.500000	0.500613	0.500271	0.501004	0.500000	0.513198	0.819447	1.132533	1.446029	1.751310
	λ=0.62	0.500004	0.500003	0.500001	0.500000	0.500000	0.500000	0.500000	0.500818	0.500000	0.500000	0.500000	0.500002	0.671861	0.995425	1.399176	1.796302	2.083441
	λ=0.64	0.500122	0.500059	0.500020	0.500000	0.500007	0.500161	0.500030	0.500047	0.500000	0.500208	0.500229	0.566847	0.900380	1.286944	1.600419	1.985458	2.369062
	λ=0.66	0.500000	0.500000	0.500076	0.500305	0.500539	0.500780	0.501020	0.501267	0.501526	0.501779	0.524393	0.753060	1.138209	1.551825	1.969741	2.388272	2.806833
	λ=0.68	0.500036	0.500040	0.500002	0.500074	0.500005	0.500028	0.500029	0.500000	0.500000	0.500000	0.649395	1.015148	1.395623	1.793233	2.159453	2.563916	2.910605
	λ=0.70	0.500002	0.500002	0.500002	0.500002	0.500002	0.500002	0.500003	0.500003	0.500005	0.559828	0.894887	1.279633	1.573891	1.943071	2.342531	2.712805	2.990566
	λ=0.72	0.530452	0.525919	0.519106	0.512153	0.508439	0.502584	0.500000	0.500000	0.500000	0.500000	0.500000	0.500000	0.500000	0.725195	0.500000	0.505897	0.513113
	λ=0.74	0.503904	0.501525	0.500809	0.500887	0.501142	0.500589	0.500365	0.500220	0.500217	0.500026	0.500177	0.500256	0.514356	0.500138	0.500089	0.500033	0.504105
	λ=0.76	0.500115	0.500078	0.500073	0.500047	0.500050	0.500048	0.500017	0.500033	0.500000	0.500000	0.500000	0.500001	0.540637	0.500000	0.500000	0.500000	0.500301
	λ=0.78	0.500005	0.500001	0.500001	0.500021	0.500076	0.500016	0.500000	0.500000	0.500056	0.500000	0.500000	0.500000	0.500009	0.528789	0.500019	0.500000	0.500000
	λ=0.80	0.501094	0.500593	0.500131	0.500024	0.500000	0.500019	0.500071	0.500266	0.500031	0.500000	0.500000	0.500000	0.500001	0.509774	0.500152	0.500254	0.510217
	λ=0.82	0.507517	0.506337	0.505176	0.503779	0.502516	0.501039	0.500000	0.500000	0.500000	0.500000	0.500005	0.500578	0.522289	0.500023	0.500000	0.500005	0.502345
	λ=0.84	0.500294	0.500212	0.500163	0.500130	0.500077	0.500131	0.500000	0.500000	0.500000	0.500000	0.500000	0.519251	0.531961	0.500000	0.500000	0.501028	0.511632
	λ=0.86	0.500000	0.500208	0.500358	0.500184	0.500000	0.500571	0.501113	0.501184	0.500000	0.500000	0.500000	0.500000	0.500025	0.500013	0.500000	0.500910	0.505425
	λ=0.88	0.507033	0.505233	0.504195	0.503121	0.502048	0.500903	0.500000	0.500000	0.500000	0.500000	0.500024	0.502552	0.500000	0.500000	0.500000	0.500000	0.503791
	λ=0.90	0.505498	0.504241	0.503342	0.502601	0.501586	0.500829	0.500002	0.500010	0.500000	0.500001	0.500416	0.506458	0.500071	0.500004	0.500000	0.500000	0.502213
	λ=1.00	0.501411	0.500824	0.500616	0.500354	0.500001	0.500036	0.500129	0.500061	0.500000	0.500000	0.500000	0.500001	0.506596	0.500000	0.500000	0.500061	0.502091
	λ=1.10	0.511484	0.509052	0.506610	0.504515	0.502397	0.500145	0.500000	0.500000	0.500048	0.500054	0.500026	0.500035	0.500000	0.500000	0.500000	0.503696	0.510212
	λ=1.20	0.503963	0.503251	0.502623	0.502092	0.501841	0.501060	0.500591	0.500209	0.500000	0.500032	0.500064	0.607489	0.500000	0.500001	0.500004	0.503011	0.504249
	λ=1.30	0.505461	0.505248	0.504723	0.503660	0.502254	0.500672	0.500107	0.500034	0.500008	0.500008	0.500010	0.529019	0.500062	0.500000	0.500000	0.500321	0.504210
	λ=1.40	0.504751	0.502924	0.501673	0.500880	0.500185	0.500001	0.500015	0.500000	0.500001	0.500088	0.501920	0.509214	0.500000	0.500000	0.500061	0.500626	0.505022
	λ=1.50	0.502357	0.502174	0.501923	0.501542	0.501049	0.500161	0.500000	0.500015	0.500538	0.501025	0.501106	0.500004	0.500000	0.500006	0.503053	0.506146	0.510600
	λ=1.60	0.510433	0.506459	0.503695	0.501951	0.500868	0.500268	0.500000	0.500001	0.500004	0.505136	0.504062	0.500007	0.500001	0.500103	0.500386	0.502460	0.504703
	λ=1.70	0.506118	0.503678	0.501997	0.500969	0.500129	0.500111	0.500001	0.500000	0.500179	0.502967	0.500610	0.500107	0.500005	0.500320	0.501134	0.504227	0.507851
	λ=1.80	0.506419	0.503306	0.501279	0.500598	0.500202	0.500068	0.500000	0.500122	0.501354	0.529656	0.513726	0.500060	0.500000	0.500689	0.502169	0.504537	0.508112
	λ=1.90	0.500300	0.500000	0.500295	0.500171	0.500460	0.500121	0.500000	0.500000	0.506655	0.514125	0.500000	0.500125	0.500000	0.500705	0.500964	0.504128	0.504867
	λ=2.00	0.511390	0.507578	0.504408	0.501916	0.500472	0.500250	0.500000	0.500001	0.500004	0.500283	0.500032	0.500018	0.500004	0.500243	0.500469	0.502925	0.503425
$w_{opt}(x/L)/(2w_{min})$ [-]	**λ=0.50**	0.500000	0.500000	0.500000	0.500000	0.500000	0.500000	0.500000	0.500000	0.500000	0.500000	0.500000	0.500000	0.500000	0.500000	0.500000	0.500000	0.500000
	λ=0.52	0.500000	0.500000	0.500000	0.500000	0.500000	0.500000	0.500000	0.500000	0.500000	0.500000	0.500000	0.500000	0.500000	0.500000	0.500000	0.500000	0.500000
	λ=0.54	0.500000	0.500000	0.500000	0.500000	0.500000	0.500000	0.500000	0.500000	0.500000	0.500000	0.500000	0.500000	0.500000	0.500000	0.500000	0.500000	0.500000
	λ=0.56	0.500000	0.500000	0.500000	0.500000	0.500000	0.500000	0.500000	0.500000	0.500000	0.500000	0.500000	0.500000	0.500000	0.500000	0.500000	0.500000	0.500000
	λ=0.58	0.500000	0.500000	0.500000	0.500000	0.500000	0.500000	0.500000	0.500000	0.500000	0.500000	0.500000	0.500000	0.500000	0.500000	0.500000	0.500000	0.500000
	λ=0.60	0.500000	0.500000	0.500000	0.500000	0.500000	0.500000	0.500000	0.500000	0.500000	0.500000	0.500000	0.500000	0.500000	0.500000	0.500000	0.500000	0.500000
	λ=0.62	0.500000	0.500000	0.500000	0.500000	0.500000	0.500000	0.500000	0.500000	0.500000	0.500000	0.500000	0.500000	0.500000	0.500000	0.500000	0.500000	0.500000
	λ=0.64	0.500000	0.500000	0.500000	0.500000	0.500000	0.500000	0.500000	0.500000	0.500000	0.500000	0.500000	0.500000	0.500000	0.500000	0.500000	0.500000	0.500000
	λ=0.66	0.500000	0.500000	0.500000	0.500000	0.500000	0.500000	0.500000	0.500000	0.500000	0.500000	0.500000	0.500000	0.500000	0.500000	0.500000	0.500000	0.500000
	λ=0.68	0.500000	0.500000	0.500000	0.500000	0.500000	0.500000	0.500000	0.500000	0.500000	0.500000	0.500000	0.500000	0.500000	0.500000	0.500000	0.500000	0.500000
	λ=0.70	0.500000	0.500000	0.500000	0.500000	0.500000	0.500000	0.500000	0.500000	0.500000	0.500000	0.500000	0.500000	0.500000	0.500000	0.500000	0.500000	0.500000
	λ=0.72	2.486206	2.335240	2.214563	2.064791	1.900044	1.733582	1.566790	1.399627	1.234231	1.072753	0.942904	0.798894	0.672615	0.573016	0.500000	0.500000	0.502832
	λ=0.74	2.105540	1.961115	1.801499	1.635175	1.468541	1.306573	1.142004	0.977536	0.811945	0.651553	0.524631	0.516157	0.572549	0.504165	0.500249	0.500000	0.505198
	λ=0.76	2.135392	1.967929	1.800469	1.633047	1.465719	1.298333	1.130973	0.963746	0.797395	0.637356	0.515050	0.519618	0.630445	0.514700	0.500000	0.500013	0.544838
	λ=0.78	2.063251	1.898164	1.733049	1.567801	1.402382	1.237646	1.072616	0.908090	0.743082	0.589429	0.500000	0.500015	0.500007	0.556185	0.500295	0.500000	0.580256
	λ=0.80	2.005186	1.846515	1.687055	1.524539	1.361706	1.198405	1.035104	0.871750	0.710820	0.563334	0.500300	0.500000	0.500000	0.506971	0.500001	0.500585	0.572249
	λ=0.82	2.107516	1.945021	1.780861	1.616672	1.449945	1.282864	1.115518	0.948325	0.782328	0.623882	0.510773	0.611914	0.727449	0.602140	0.500029	0.528883	0.650266
	λ=0.84	1.998610	1.834567	1.670206	1.505693	1.341245	1.176229	1.012121	0.847832	0.689704	0.578361	0.541750	0.548214	0.500005	0.500000	0.500000	0.514101	0.609642
	λ=0.86	1.912075	1.750713	1.589992	1.431293	1.272527	1.110015	0.948499	0.789957	0.638002	0.521084	0.534330	0.584882	0.500033	0.500011	0.500000	0.524128	0.634078
	λ=0.88	2.006288	1.850041	1.686214	1.521413	1.355234	1.188111	1.020832	0.853972	0.690402	0.547568	0.500464	0.552072	0.500000	0.500000	0.500000	0.576830	0.714228
	λ=0.90	1.893805	1.740435	1.583167	1.423923	1.265173	1.103912	0.942382	0.776594	0.617412	0.500115	0.500400	0.566194	0.500068	0.500040	0.500000	0.573355	0.709594
	λ=1.00	1.737212	1.584930	1.429741	1.274715	1.119841	0.962814	0.805912	0.651987	0.518579	0.500056	0.500000	0.500080	0.531026	0.500034	0.500012	0.612896	0.759307
	λ=1.10	1.862663	1.706634	1.547644	1.383458	1.216979	1.050034	0.883004	0.718402	0.569451	0.500034	0.500121	0.500026	0.500001	0.500058	0.590834	0.744971	0.900384
	λ=1.20	1.644788	1.490465	1.334939	1.178171	1.019517	0.862646	0.704927	0.559141	0.500018	0.500103	0.500164	0.558307	0.500042	0.500047	0.592814	0.735921	0.890658
	λ=1.30	1.647002	1.486075	1.326549	1.168814	1.011275	0.852755	0.691018	0.547861	0.500056	0.500001	0.500057	0.570515	0.500004	0.511960	0.642417	0.803615	0.952690
	λ=1.40	1.590846	1.441333	1.286715	1.128474	0.969113	0.807203	0.647410	0.515386	0.500004	0.500093	0.504738	0.518663	0.500117	0.525089	0.660757	0.821449	0.965747
	λ=1.50	1.646642	1.479580	1.312668	1.145999	0.979956	0.813846	0.652930	0.521723	0.500134	0.512024	0.530151	0.500977	0.500000	0.560938	0.707576	0.862525	1.011171
	λ=1.60	1.553503	1.413714	1.264705	1.106938	0.945144	0.781156	0.626385	0.520637	0.500980	0.500015	0.502049	0.500027	0.500027	0.577415	0.727512	0.885273	1.041942
	λ=1.70	1.513729	1.367744	1.215103	1.057728	0.898686	0.736202	0.584177	0.500795	0.501166	0.533870	0.554166	0.500079	0.500000	0.578759	0.730245	0.879914	1.025966
	λ=1.80	1.524384	1.379491	1.225581	1.063090	0.899219	0.734943	0.583001	0.500101	0.501013	0.532972	0.500099	0.500054	0.500073	0.600951	0.754402	0.909755	1.057878
	λ=1.90	1.504948	1.345299	1.183268	1.022071	0.860089	0.702771	0.559475	0.510180	0.518363	0.558302	0.500046	0.500000	0.500000	0.595728	0.750141	0.897768	1.054546
	λ=2.00	1.420197	1.286003	1.144294	0.996725	0.842167	0.684355	0.546916	0.510474	0.500002	0.501961	0.500351	0.501820	0.500178	0.607071	0.762107	0.912464	1.069657

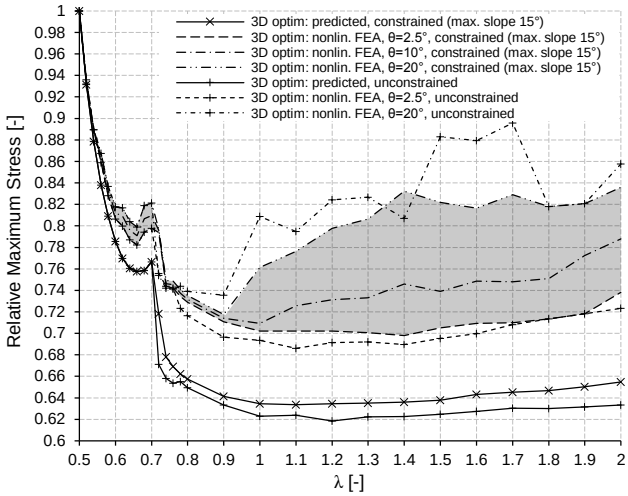

Figure 12. Plots showing predicted relative maximum stress as per Eq. 20 vs. rotated angle 'θ_z', for $\lambda \in [0.5, 2]$.

As shown in Fig. 12, the FEA results are in good agreement with the predictions. This fact corroborates the assumptions and mathematical formulation adopted in the optimization. For $\lambda \in [0.5, 0.7]$, i.e. the 'λ' range for which the optimized leaf-springs exhibit a constant width, there is a discrepancy between the FEA results and the predictions of about 2%. On the other hand, for $\lambda \in (0.7, 2]$ the optimized leaf-springs vary in both thickness and width (predominantly)—therefore deviating from a constant cross section leaf-spring even further than in the previous case— and the discrepancy is about 6%. These discrepancies, which in reality are smaller as the lowest FEA line shown in Fig. 12 corresponds to θ_z=2.5° instead of θ_z=0°, are in any case in line with the error estimates given by Timoshenko[13] for those instances where linear bending theory is applied to beams of small taper. Furthermore, the fact that the formulation adopted for the optimization only considers the stresses arising from bending, unlike the FEA performed which additionally accounts for axial and shear stresses, geometrical nonlinearity effects, etc. also contributes to these discrepancies between the predicted and the FEA results.

As the finite element analysis shows, for small angles of rotation 'θ_z' very significant stress reductions are achievable, of up to as much as 30% in the case of the AGF mechanism ($\lambda \approx 1$). These results are of great practical transcendence. Not only because of the significance of the stress reductions possible, but also because of the many crossed flexure pivots of $\lambda > 0.7$ such as the cartwheel hinge[27], the 'butterfly' flexure pivot[28], the compound generalized cross-spring pivot[12,29], the anti-symmetric double leaf-type isosceles-trapezoidal flexure (ADLIF)[30], etc. that could benefit from these stress reductions simply by WEDM-ing their width profile to the corresponding optimum. The only case for which shape optimization yields no stress reduction is λ=0.5. This means that a constant cross section leaf-spring is already the optimal shape for that particular pivot configuration. As the angle of rotation 'θ_z' increases, the stress reduction capability of the optimized leaf-springs is largely retained for $\lambda \leq 0.9$. For $\lambda > 0.9$, however, this capability deteriorates with 'θ_z' as shown in

In the light of the above results, it is remarkable that the optimization approach employed —which is based on a linear formulation and therefore theoretically valid only for small angles of rotation—, yields optimized leaf-springs which, for most of the 'λ' range analysed, largely retain their stress reduction potential even at large deflection angles 'θ_z' for which a non-linear theory would otherwise have been required. This would go to suggest, as Eq. 17 states, that for all practical purposes the optimized leaf-spring shapes are unique for the whole 'θ_z' domain, or in other words, independent of 'θ_z'. Obviously, this is strictly speaking not true. As the FEA results corresponding to the unconstrained optimization leaf-springs show, in reality the optimum shape of a leaf-spring is indeed dependent upon the angle of rotation 'θ_z'. Indeed, as illustrated in Fig. 12, it is possible to have two different thickness profiles such that one is 'optimum' (i.e. yields the lowest stress) from θ_z=0° up to a certain value of 'θ_z', while the other is 'optimum' from the aforementioned 'θ_z' value onwards. In any case, the truly important fact is that constrained optimization (as defined in Section 2.2) yields leaf-springs whose maximum stress reduction capability is not only very close to that of those resulting from unconstrained optimization, but, furthermore, most uniform over the 'θ_z' domain. This advantage, added to the fact that constrained optimization guarantees that the optimized profiles will have the same stress reduction capability when scaled to other absolute dimensions, supports even further the optimization approach adopted in this work based on a linear formulation and with geometric constraints set upon the target optimized leaf-springs.

4. CONCLUSIONS

The objective of the present study was to investigate the potential for stress reduction through shape optimization as applied to distributed compliance leaf-type springs in crossed flexure pivots of $\lambda_{i,j} \in [-1, 2]$.

When performing a stress optimization on these types of slender mechanical members (i.e. $L/t_{min}>25$), it has been proven through FEA validation that the stress field may be satisfactorily predicted by employing a linear strain energy formulation, provided that the angular deflection is small (i.e. $\theta_z \leq 15º$) and that the slope of the resulting width profile is constrained (i.e. $dz/dx \leq \tan 15°$).

The shape of the optimized leaf-springs was parametrically defined by 'n' evenly spaced interpolation points, whose 'y' and 'z' coordinates determine the thickness and width profiles of the optimized leaf-springs respectively. It was found that n=17 yields the best compromise between size/complexity of the polynomials defining the optimized profiles and achieved stress reduction.

The resulting optimized leaf-springs are proven to be not only independent of the angular rotation at which the pivot operates (i.e. θ_z) and the material of the leaf-springs (i.e. E), but also linearly scalable to leaf-springs of any length (i.e. L), minimum thickness (i.e. t_{min}) and minimum width (i.e. w_{min}).

Validated using non-linear finite element analysis, the results show very significant stress reductions relative to pivots with constant cross section leaf-springs, of up to as much as 30% for the specific pivot configuration employed in the AGF mechanism ($\lambda \approx 1$). For $\lambda \in [0.5, 0.7]$, the optimized leaf-springs exhibit only a thickness profile variation (and a constant width profile). Conversely, for $\lambda \in (0.7, 2]$ the optimized leaf-spring exhibit a tangible width variation yet very subtle thickness changes, therefore suggesting that virtually the same stress reductions could have been obtained simply by optimizing the width while leaving the thickness constant. The only case for which no stress reduction was feasible — therefore implying that a constant cross section leaf-spring is already optimal— was $\lambda=0.5$.

For $\lambda \in [0.5, 0.9]$ the optimized leaf-springs largely retain their stress reduction potential even at angles of rotation as high as $\theta_z=20º$ (i.e. even outside the range where linear formulations are applicable). For the rest of the 'λ' range analysed, however, the stress reduction potential of the optimized leaf-springs degrades slightly as the angle of rotation increases.

It can be concluded that shape optimization offers great potential for reducing the stress of crossed flexure pivots and therefore, for extending their fatigue life and/or rotational range.

Future work will explore the potential to further reduce stress in the AGF's flexural pivots by performing a parametric optimization of the mechanism as a whole. To that end, the specific in-flight loading and blade deflection conditions will be considered, in order to calculate the optimum number of leaf-springs to be employed, their relative position along the flap's span, as well as their individual widths.

ACKNOWLEDGEMENTS

This project is funded by the Clean Sky Joint Technology Initiative (JTI) (topic JTI-CS-2010-4-GRC-01-005), which is part of the European Union's 7th Framework Programme (FP7/2007-2013).

REFERENCES

[1] Clean Sky website - Green Rotorcraft - Blades (GRC1) - Techno streams, <http://www.cleansky.eu/content/page/innovative-rotor-blades-technology-streams> (23 January 2013).
[2] Freire Gómez, J., Booker, J. D. and Mellor P. H., "Design and development of an active Gurney flap for rotorcraft," Proc. SPIE 8690, 86900F (2013).
[3] Howell, L. L., Magleby, S. P. and Olsen, B. M., [Handbook of Compliant Mechanisms], Wiley, (2013).
[4] Loendersloot, R., Freire Gómez, J. and Booker, J. D., "Wind tunnel testing of a full scale helicopter blade section with an upstream active Gurney flap," Proc. European Rotorcraft Forum, (2014).
[5] Hoff, S. C. van't, and Tuinstra, M., "Time-resolved stereo PIV measurements of an active Gurney flap system," Proc. European Rotorcraft Forum, (2014).

[6] Xu, P., Jingjun, Y., Guanghua, Z. and Shusheng, B., "An effective pseudo-rigid-body method for beam-based compliant mechanisms," Precision Engineering 34(3), 634–639 (2010).
[7] Oiwa, T. and Sugimoto, T., "Shape Optimization for Flexure Hinges," Journal of the Japan Society for Precision Engineering 63, 1454–1458, (1997).
[8] Bona, F. D., and Munteanu, M. G., "Optimized Flexural Hinges for Compliant Micromechanisms," Analog Integrated Circuits and Signal Processing 44(2), 163–174, (2005).
[9] Zelenika, S., Munteanu, M. G. and Bona, F. D., "Optimized flexural hinge shapes for microsystems and high-precision applications," Mechanism and Machine Theory 44(10), 1826–1839, (2009).
[10] Zhu, B., Zhang, X. and Fatikow, S., "Design of single-axis flexure hinges using continuum topology optimization method," Science China Technological Sciences 57(3), 560–567, (2014).
[11] Hongzhe, Z., and Shusheng, B., "Stiffness and stress characteristics of the generalized cross-spring pivot," Mechanism and Machine Theory 45(3), 378–391, (2010).
[12] Hongzhe, Z., and Shusheng, B., "Accuracy characteristics of the generalized cross-spring pivot," Mechanism and Machine Theory 45(10), 1434–1448, (2010).
[13] Gere, J. M. and Timoshenko, S. P., [Mechanics of Materials], Brooks/Cole Engineering Division, (1984).
[14] Xu, P., Jingjun, Y., Guanghua, Z., Shusheng, B. and Zhiwei, Y., "Analysis of rotational precision for an isosceles-trapezoidal flexural pivot," Journal of Mechanical Design 130(5), 052302, (2008).
[15] Haringx, J. A., "The cross-spring pivot as a constructional element," Applied Scientific Research 1(1), 313–332, (1949).
[16] Wittrick, W. H., "The properties of crossed flexure pivots and the influence of the point at which the strips cross," Aeronautical Quaterly 2(4), 272–292, (1951).
[17] Wittrick, W. H., "The theory of symmetrical crossed flexure pivots," Australian Journal of Scientific Research, Series A: Physical Sciences 1, 121-134, (1948).
[18] Hongzhe, Z., Shusheng, B., and Jingjun, Y., "Nonlinear deformation behavior of a beam-based flexural pivot with monolithic arrangement," Precision Engineering 35(2), 369–382, (2011).
[19] Shusheng, B., Yanbin, Y., Shanshan, Z., and Jingjun, Y., "Modeling of cross-spring pivots subjected to generalized planar loads," Chinese Journal of Mechanical Engineering 25(6), 1075–1085, (2012).
[20] Xu, P., Jingjun, Y., Guanghua, Z., and Shusheng, B., "The stiffness model of leaf-type isosceles-trapezoidal flexural pivots," Journal of Mechanical Design 130(8), 082303, (2008).
[21] Lobontiu, N., [Compliant Mechanisms: Design of Flexure Hinges], CRC Press, (2003).
[22] Madou, M. J., [Fundamentals of Microfabrication and Nanotechnology], CRC Press, (2011).
[23] Saile, V., Wallrabe, U., Tabata, O., Korvink, J. G., Brand, O., Fedder, G. K. et al., [LIGA and its Applications (Advanced Micro and Nanosystems)], Wiley-VCH, (2009).
[24] Fritsch, F. and Carlson, R., "Monotone Piecewise Cubic Interpolation," SIAM Journal on Numerical Analysis 17(2), 238–246, (1980).
[25] Kahaner, D., Moler, C. and Nash, S., [Numerical Methods and Software], Prentice Hall, (1988).
[26] MathWorks, <http://www.mathworks.co.uk/products/matlab/> (04 April 2014).
[27] Smith, S. T., [Flexures: Elements of Elastic Mechanisms], CRC Press, (2000).
[28] Henein, S., Spanoudakis, P., Droz, S., Myklebust, L. I. and Onillon, E., "Flexure pivot for aerospace mechanisms," Proc. 10th European Space Mechanisms and Tribology Symposium, (2003).
[29] Hongzhe, Z., Shusheng, B. and Jingjun, Y., "A novel compliant linear-motion mechanism based on parasitic motion compensation," Mechanism and Machine Theory 50, 15–28, (2012).
[30] Xu, P. and Yu, J., "ADLIF: a new large-displacement beam-based flexure joint," Mechanical Sciences 2, 183–188, (2011).
[31] Zelenika, S. and Bona, F. D., "Analytical and experimental characterisation of high-precision flexural pivots subjected to lateral loads," Precision Engineering 26(4), 381–388, (2002).